Supplementary Table 1 | X-ray and cryo-EM data collection and refinement statistics.

a

	CTB1 SAT-KS-MAT
Data collection	
Space group	$C222_1$
Cell dimensions	
a, b, c (Å)	108.05, 230.2, 253.8
α, β, γ (°)	90.0, 90.0, 90.0
Resolution (Å)	126.9 – 2.77
R_{merge} (%)*	21.2 (193.8)
$I/\sigma I$*	10.13 (1.03)
$CC_{1/2}$*	99.5 (43.3)
Completeness (%)*	99.2 (91.9)
Redundancy*	8.5 (5.6)
Refinement	
Resolution (Å)	63.45 – 2.77
R_{work}/ R_{free}	0.21 / 0.24
No. atoms	39,201
Protein	38,682
Ligand/ion	167
Water	352
B-factors	70.17
Protein (Å^2)	70.31
Ligand/ion (Å^2)	84.20
Water (Å^2)	48.78
R.m.s deviations	
Bond lengths (Å)	0.002
Bond angles (°)	0.496

b

	CTB1 SAT°-KS-MAT°=ACP2
Data collection and processing	
Nominal magnification	105,000x
Voltage (keV)	300
Electron exposure (e- Å^{-2}) initial / final	90 / 41
Defocus range(μm)	0.8-4.5
Pixel size (Å)	1.326
Symmetry imposed	C1
Movies	1,728
Frames per movie	60
Initial particles images	122,089
Final particle images	25,107
Refinements	
Initial model used	ab initio
Model resolution (Å)	7.1
FSC threshold	0.143
Model resolution range(Å)	4-10
Map sharpening B-factor (Å^2)	-350
Model composition	
Non-hydrogen atoms	19,628
Protein residues	2,591
Ligands	0
R.m.s deviations	
Bond lengths (Å)	0.010
Bond angles (°)	1.290
Validation	
MolProbity score	1.57
All-atom clashscore	6.09
Rotamer outliers (%)	0.00
Ramachandran plot	
Favored (%)	96.47
Allowed (%)	3.41
Disallowed (%)	0.12

(a) Crystallographic data collection and refinement statistics. The resolution cutoff was determined by $CC_{1/2}$ criterion (Karplus, P. A. & Diederichs, K. Science 336, 1030-1033 (2012)). *, Highest resolution shell is shown in parentheses. **(b)** Cryo-electron microscopic data collection and refinement statistics.

Supplementary Table 2 | Structural comparison and interface analysis of CTB1 SAT-KS-MAT.

a

Structure 1	Structure 2	C_α r.m.s.d. [Å]	Aligned residues
CTB1 SAT	CTB1 SAT (2nd chain)	0.34	350
	Closest* in PDB (3G87) no multienzyme	2.56	262
	human FAS MAT (3HHD)	2.59	249
	CazM SAT (4RPM) loading domain	2.63	272
	PksE AT (5DZ7)†	2.64	245
	procine FAS MAT (2VZ9)	2.65	244
	PKS13 AT (3TZX)	2.75	249
	PksC AT (5DZ6) †	2.78	251
	CTB1 MAT	2.81	255
	DEBS AT_5 (2HG4)	2.81	254
	CurL AT (4MZ0)	2.83	251
	DEBS AT_3, (2QO3)	2.86	261
	DisD AT (3RGI)†	2.87	258
	VinK (5CZD)	2.87	242
	AVES1 AT (4RL1) loading domain	2.89	256
	ZmaA (4QBU)	3.01	244
	DYNE8 AT (4AMP)	3.05	217
	MAS-like AT (5BP1)	3.18	259
	OzmQ partial AT (4OQJ)	3.22	92
CTB1 KS	CTB1 KS (2nd chain)	0.23	435
	PksL KS (5ENY)	1.40	392
	C0ZGQ5 KS (4Z37)	1.40	398
	CurL KS (4MZ0)	1.41	400
	MgsF KS (4TKT)†	1.41	401
	PksJ KS (4NA3)†	1.42	404
	human FAS KS (3HHD)	1.44	389
	procine FAS KS (2VZ9)	1.48	388
	DEBS KS_3, (2QO3)	1.49	406
	DEBS KS_5 (2HG4)	1.49	392
	MgsE KS (4QYR)†	1.52	400
	OzmH KS0 (4OPF)†	1.52	339
	MAS-like KS (5BP1)	1.55	347
	OzmN KS (4WKY)†	1.60	374
	RhiE KS (4KC5)†	1.61	399
	Closest* - FabF KS (4JB6) no multienzyme	1.64	378
	OzmQ (4OQJ)†	1.75	375
CTB1 MAT	CTB1 MAT (2nd chain)	0.23	304
	CurL AT (4MZ0)	1.72	281
	MAS-like AT (5BP1)	1.82	285
	PKS13 AT (3TZY)	1.83	290
	human FAS MAT (3HHD)	1.83	280
	procine FAS MAT (2VZ9)	1.85	279
	DYNE8 AT (4AMP)	1.86	231
	DEBS AT_3, (2QO3)	1.87	285
	DEBS AT_5 (2HG4)	1.89	290
	Closest* in PDB: AVES1 AT (4RL1) loading domain	1.92	284
	ZmaA (4QBU)	2.00	275
	DisD AT (3RGI)†	2.02	269
	PksC AT (5DZ6)†	2.06	266
	PksE AT (5DZ7)†	2.09	264
	VinK (5CZD)	2.26	261
	OzmQ partial AT (4OQJ)	2.50	89
	CazM SAT (4RPM) loading domain	2.68	252

b

Interface 1	Interface 2	Min area [Å^2]	Max area [Å^2]	Hydrogen bonds	Salt bridges
SAT	KS-LD-MAT-post MAT linker	1197.2	1230.1	6-8	3
SAT[§]	KS[§]	183.8	184.9	1-2	0
SAT[§]	MAT[§]	946.1	966.8	5-6	2-3
SAT	SAT	323.7	323.7	0	0
SAT dimer	KS dimer	659.9	659.9	3	0
SAT dimer	KS-LD-MAT-post MAT linker dimer	2718.5	2718.5	14	7
SAT[§]	SAT-KS linker[§]	486.7	500.1	1-2	0
KS	KS	2607.1	2607.1	10	1
KS	LD	415.9	416.5	4	2
KS	post-MAT linker	1460.0	1465.8	12-13	3-4
LD	post-MAT linker	1262.5	1277.4	8	0-1
MAT	post-MAT linker	908.5	911.5	4	1

(a) C_α r.m.s. deviations obtained for structural comparison of crystallized CTB1 domains with their closest structural neighbors in the PDB and of multienzyme PKSs and FASs (to the best of our knowledge). For structures with several protomers only the best matches are reported. *,Q-score based, †, *trans*-AT PKS. **(b)** Interfaces in the crystal structures of CTB1 SAT-KS-MAT. [§]Interface with the second protomer.

Supplementary Table 3 | Plasmids used in this study

Plasmid	Protein	Vector	Tag	MW (g/mol)	ε ($M^{-1}cm^{-1}$)
pECTB1-NKA6	SAT-KS-MAT	pET-24a	*C*-His_6	140150	138200
pECTB1-SKM-C119A-S1010A	SAT°-KS-MAT°	pET-24a	*C*-His_6	140150	138200
p28CTB1-ACP1	ACP1	pET-28a	*N*-His_6	11160	N/A
p28CTB1-ACP2	ACP2	pET-28a	*N*-His_6	11970	5500
pECTB1-SKM-R461A	SAT-KS-MAT-R461A	pET-24a	*C*-His_6	140150	138200
pECTB1-SKM-R461E	SAT-KS-MAT-R461E	pET-24a	*C*-His_6	140150	138200
pECTB1-SKM-R658A	SAT-KS-MAT-R658A	pET-24a	*C*-His_6	140150	138200
pECTB1-SKM-R658E	SAT-KS-MAT-R658E	pET-24a	*C*-His_6	140150	138200
pECTB1-SKM-R879A	SAT-KS-MAT-R879A	pET-24a	*C*-His_6	140150	138200
pECTB1-SKM-R879E	SAT-KS-MAT-R879E	pET-24a	*C*-His_6	140150	138200
pECTB1-PT	PT	pET-24a	*C*-His_6	41240	26150
pECTB1-TE	TE	pET-28a	*N*-His_6	33630	38055

Supplementary Table 4 | Primers used in this study.

Primer	Sequence 5'-3'
CTB1-ACP1-5-A	ATTACATATGGCAACCCAAGTGACTCCGCAA
CTB1-ACP2-3-C	ATTAGCGGCCGCGATCTCGTTAGGGGATGGATCAGT
CTB1-ACP2-5	ATTACATATGGATCCATCCCCTAACGAGAT
CTB1-ACP2-stop-3	TAATGCGGCCGCCTATTCCGTTGACCCAGAGAACC
T7	TAATACGACTCACTATAGGG
T7-term	GCTAGTTATTGCTCAGCGG
CTB1-C119A-5	TGCATTACCGGCGTTGCAACCGGCGCA
CTB1-C119A-3	CGTCAATGCGCCGGTTGCAACGCCGGT
CTB1-S1010A-5	GGTAGTTGGCCACGCGTTGGGCGAGTATGC
CTB1-S1010A-3	GCATACTCGCCCAACGCGTGGCCAACTACC
CTB1-R461A-5	ACATGAGTCCGGCGGAAGCGCCGC
CTB1-R461A-3	GCGGCGCTTCCGCCGGACTCATGT
CTB1-R461E-5	ACATGAGTCCGGAAGAAGCGCCGC
CTB1-R461E-3	GCGGCGCTTCTTCCGGACTCATGT
CTB1-R658A-5	GCCTCTATCACTGCGCCTCATGCCGGAG
CTB1-R658A-3	CTCCGGCATGAGGCGCAGTGATAGAGGC
CTB1-R658E-5	GCCTCTATCACTGAACCTCATGCCGGAG
CTB1-R658E-3	CTCCGGCATGAGGTTCAGTGATAGAGGC
CTB1-R879A-5	GAGTGCACCATGCGCACAGAGCCGTAGC
CTB1-R879A-3	GCTACGGCTCTGTGCGCATGGTGCACTC
CTB1-R879E-5	GAGTGCACCATGAACACAGAGCCGTAGC
CTB1-R879E-3	GCTACGGCTCTGTGTTCATGGTGCACTC

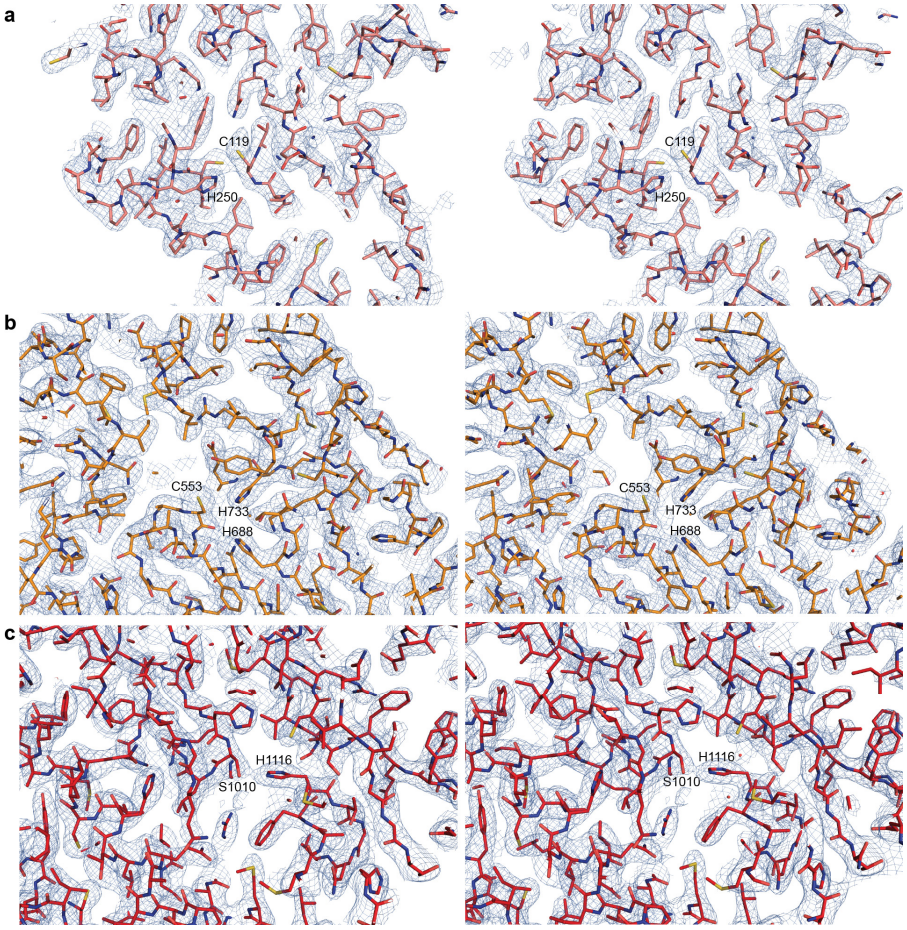

Supplementary Figure 1 | Stereo electron density quality assessment maps. $2F_o$-F_c electron density maps at 1.0 σ of the SAT (**a**), KS (**b**), and MAT (**c**) active site regions are shown.

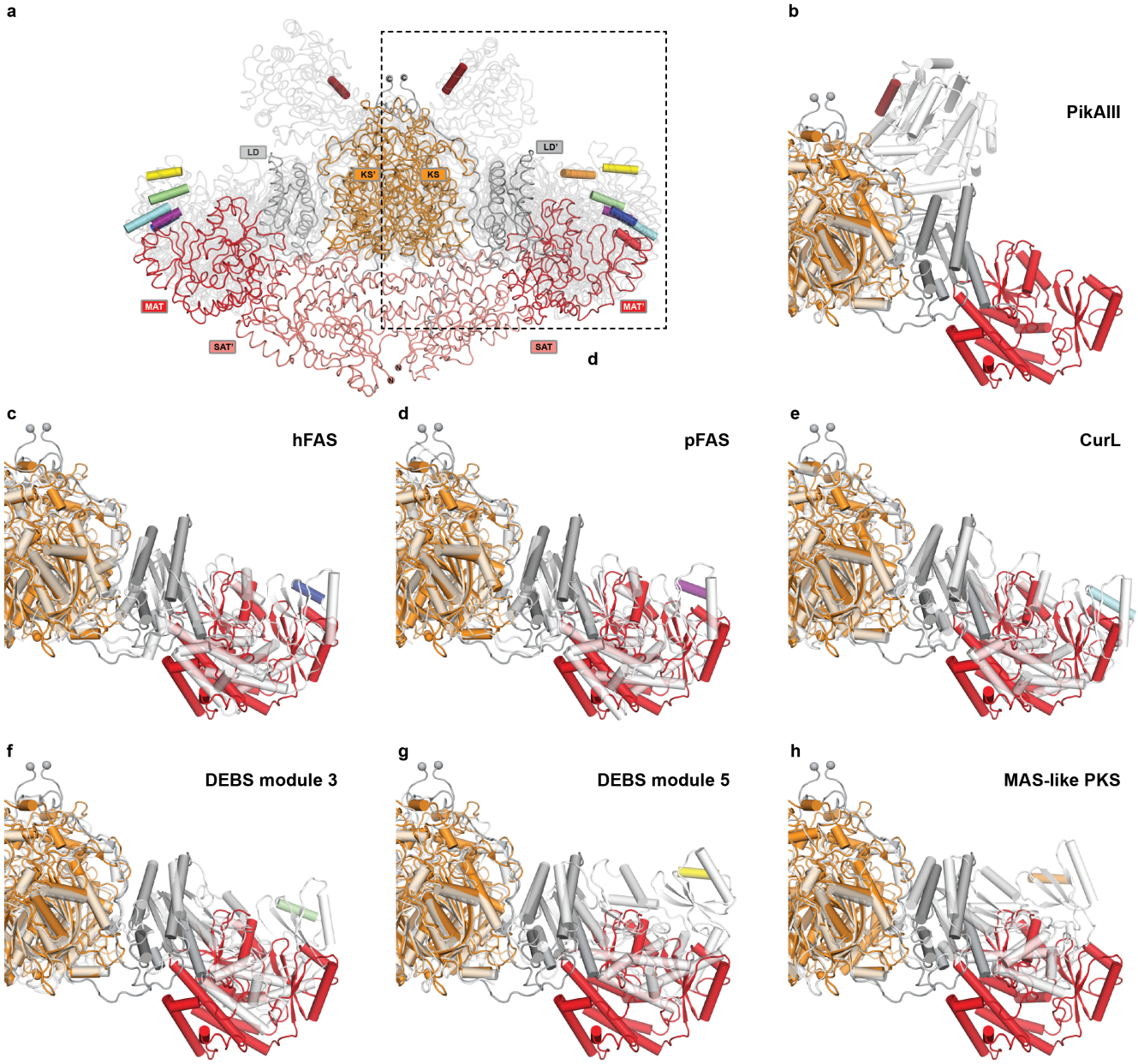

Supplementary Figure 2 | Comparison of PKS and FAS condensing region structures. (a) Overview of all superposed condensing region structures on the CTB1 KS domain. Structural differences are visualized by hinge-bending motions of the (M)ATs as described by Herbst *et al.* 2016 (Nature 531, 533-537). Colored loop representation is shown for CTB1, all other structures are shown grey transparent. Equivalent cylindrical helix of the (M)AT domains are shown to indicate structural differences relative to CTB1 (light red) for PikAIII (dark red, **b**), human FAS

(hFAS, dark blue, PDB:3hhd, **c**), porcine FAS (pFAS, PDB:2vz9, violet, **d**), CurL (cyan, PDB:4mz0, **e**), DEBS module 3 (green, PDB:2qo3, **f**), DEBS module 5 (yellow, PDB:2hg4, **g**) and a MAS-like PKS (orange, PDB:5bp1, **h**). **(b-h)** Inset of (a) in cartoon representation showing the individual superpositions. The model corresponding to PikAIII (b) was fitted according to Dutta *et al.* 2014 (Nature 510, 512-517) (EMDB:5649).

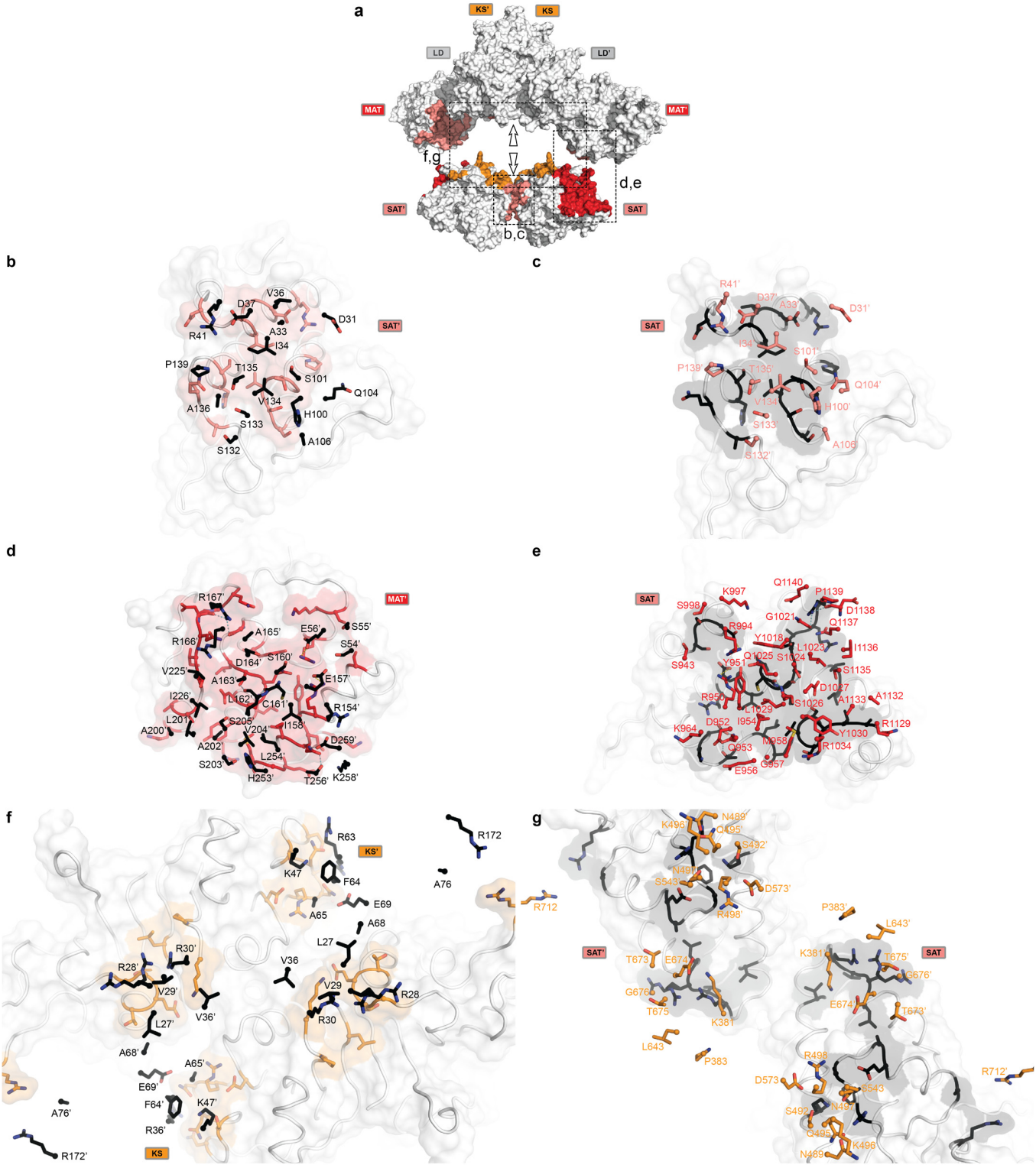

Supplementary Figure 3 | SAT interfaces in the loading/condensing region of CTB1. (a)

Overview of interfaces with insets showing the location of the SAT/SAT **(b,c)**, SAT/MAT **(d,e)**,

and SAT/KS **(f,g)** interfaces. All interfaces are shown in a top view. Transparent surfaces are colored according to interfacing residues of the domain in the back. All interfaces are shown from both sides corresponding to a 180° rotation between the left and right panel. Residue numbers correspond to interfacing residues in the front shown in the same color. Cα positions are shown as spheres. Salt bridges (yellow) and hydrogen bonds (cyan) are indicated as dotted lines.

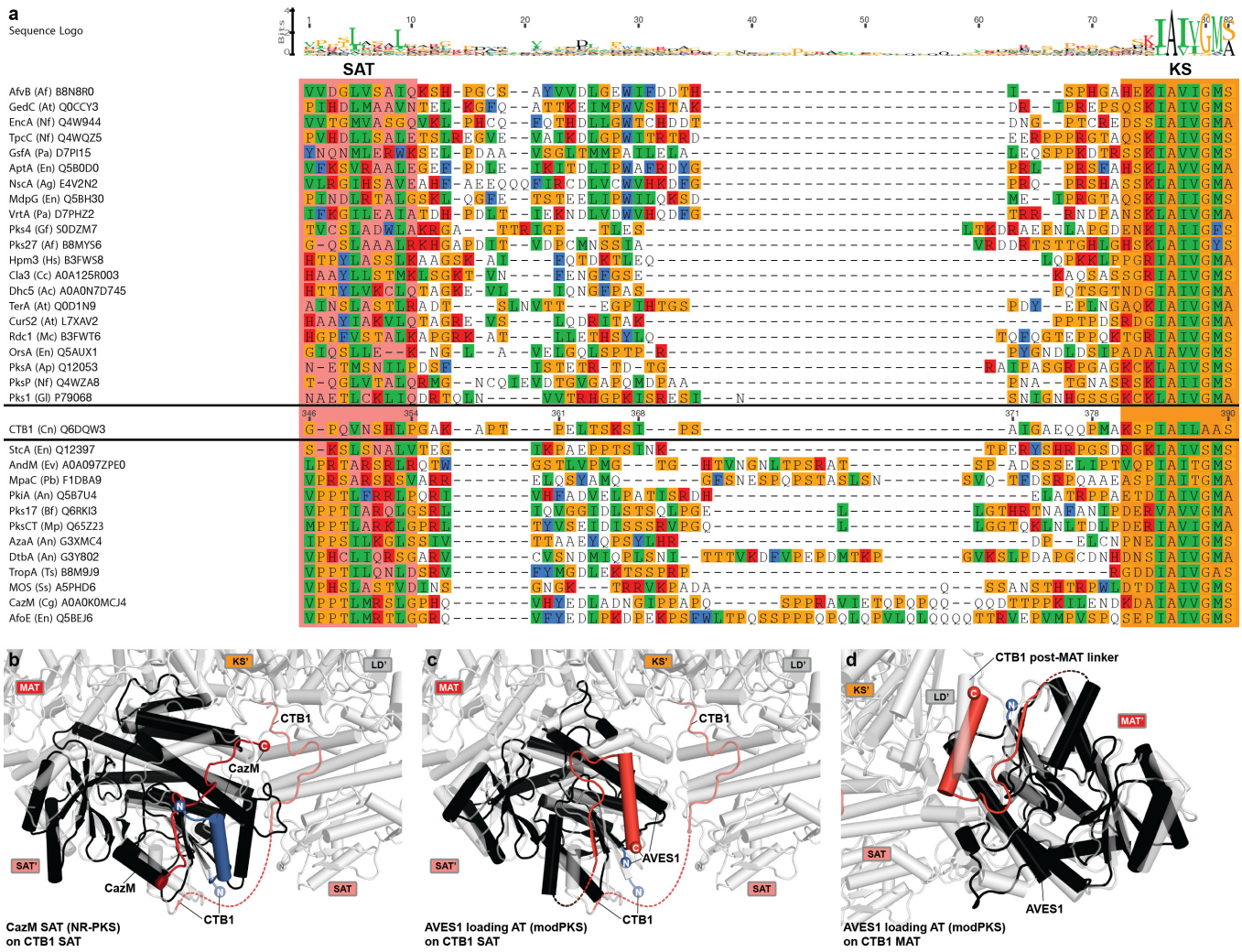

Supplementary Figure 4 | Integration of loading domains in PKS. **(a)**, Sequence alignment of 34 SAT-KS linker sequences of NR-PKS. All sequences are labelled as "protein name (organism abbreviation) Uniprot number". **(b)** Superposition of the CazM SAT (black) onto the SAT domain of CTB1 SAT-KS-MAT (light grey) shows a similar location of the SAT *C*-terminal linker ending (dark red/light red for CazM/CTB1), which points towards the *N*-terminus of the KS in CTB1. **(c)** Superposition of the loading domain of the AVES1 avermectin modPKS (black) onto the SAT domain of CTB1 SAT-KS-MAT reveals differences in C-terminal linker organization. **(d)** Superposition of the AVES1 loading domain onto CTB1 MAT shows that the

AVES1 post-loading domain linker contains an α-helix that matches the linker architecture of MAT in CTB1 (and AT domains in modPKS).

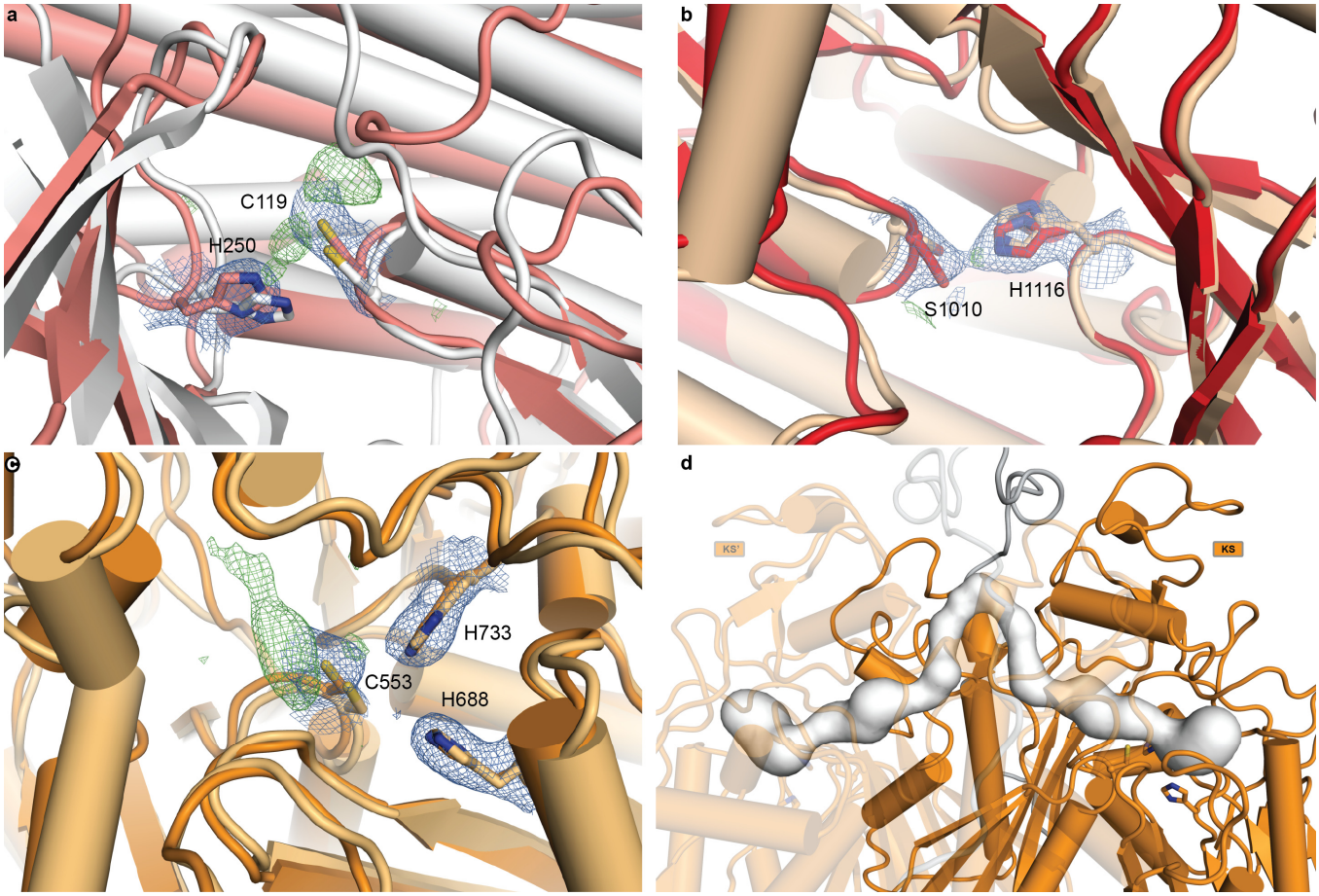

Supplementary Figure 5 | The individual active sites of SAT, MAT and KS are structurally conserved. **(a-c)** Superpositions onto previously known structures (as listed in parenthesis) of the SAT (a, pink, with CazM SAT in white), MAT (b, red, with CurL AT in wheat), and KS (c, orange, with CurL KS in light orange) domains are shown in cartoon representation. Active site residues are shown in stick representation with residue numbers corresponding to CTB1. Electron density maps for CTB1 active site residues are shown with a blue ($2F_o$-F_c at 1.0 σ) and green (F_o-F_c at 3.0 σ) mesh. Unidentified difference density around the active site residues C119 (SAT) and C553 (KS) indicated partial acylation or oxidation. **(d)** A narrow and hydrophobic active site tunnel (white) connects the KS active sites.

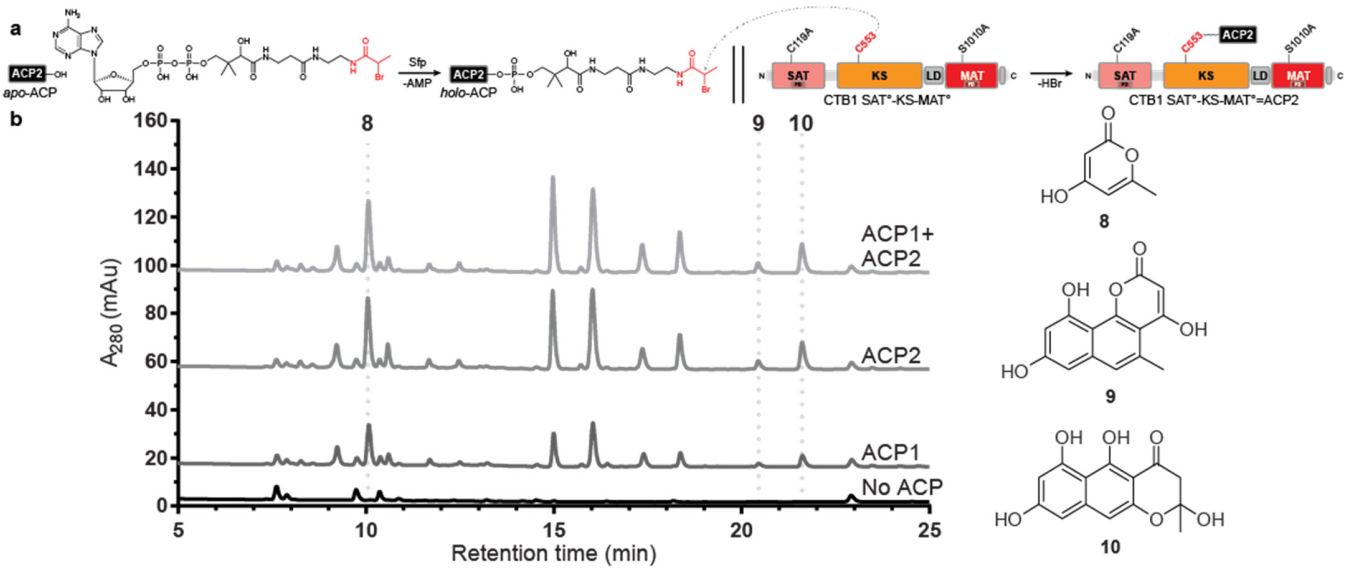
a
ACP2
apo-ACP
Sfp
-AMP
holo-ACP
C119A
C553
S1010A
SAT
KS
LD
MAT
CTB1 SAT°-KS-MAT°
-HBr
ACP2
CTB1 SAT°-KS-MAT°=ACP2
b
A280 (mAu)
Retention time (min)
ACP1+ ACP2
ACP2
ACP1
No ACP
8
9
10

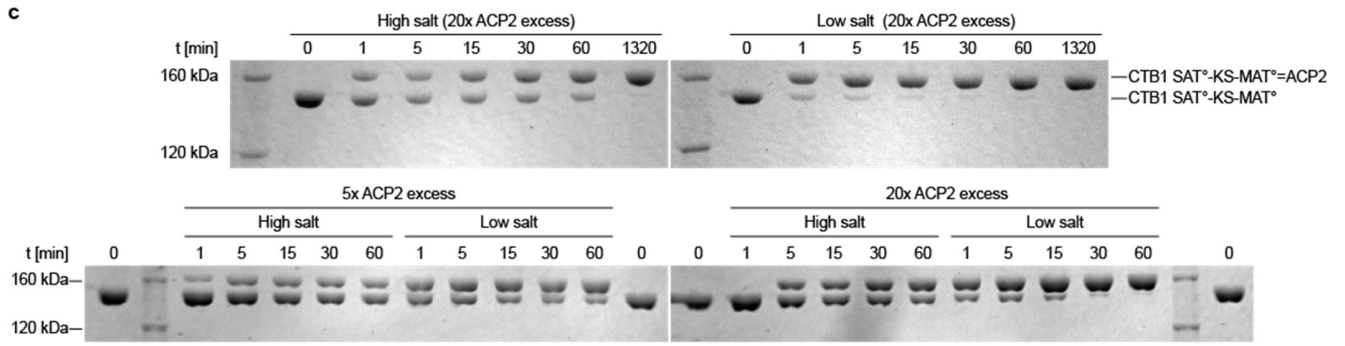
c
High salt (20x ACP2 excess)
Low salt (20x ACP2 excess)
t [min]
160 kDa
120 kDa
CTB1 SAT°-KS-MAT°=ACP2
CTB1 SAT°-KS-MAT°
5x ACP2 excess
20x ACP2 excess
High salt
Low salt

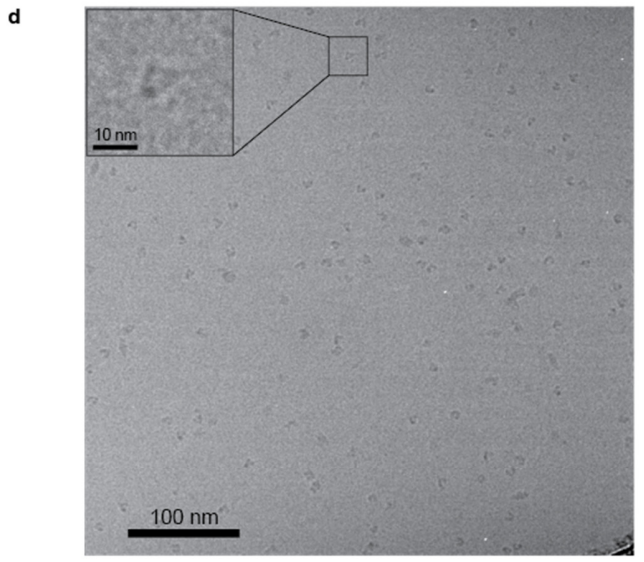
d
10 nm
100 nm

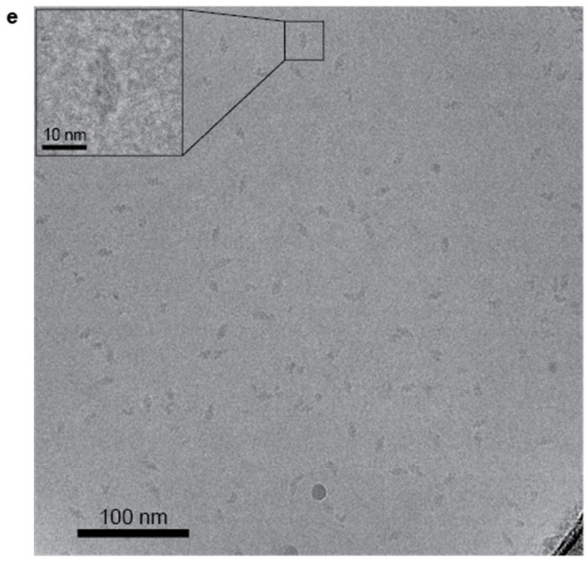
e
10 nm
100 nm

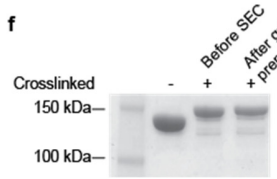
f
Before SEC
After grid preparation
Crosslinked
150 kDa
100 kDa

Supplementary Figure 6 | ACP activity, crosslinking and cryo-EM sample preparation. **(a)** Scheme for ACP2 loading with a dephospho-amino-CoA analog (black), containing the α-bromopropionyl crosslinker (red), and site specific crosslinking to the KS domain of CTB1 SAT°-KS-MAT°. **(b)** HPLC chromatograms (280 nm) of minimal *in vitro* CTB1 reconstitution reactions with SAT-KS-MAT and ACP1 (10 μM), ACP2 (10 μM), or both (5 μM each). Curves are off-set for visualization. Previously characterized CTB1 derailment products **8**, **9**, and **10**, and negative controls lacking ACP are indicated. No increase in activity is observed when ACP1 and ACP2 are combined, suggesting they are biosynthetically equivalent and interchangeable. These experiments were repeated twice with similar results. **(c)** Denaturing SDS-PAGE analysis with Coomassie staining of crosslinking time course in high (50 mM Tris pH 7.5, 250 mM NaCl) and low (50 mM Tris pH 7.5) salt buffer as well as for two different CTB1 SAT°-KS-MAT°:ACP2 ratios. Crosslinking proceeds faster in low salt buffer and at higher excess of ACP2. Gels are cropped. These experiments were repeated more than three times from independent protein preparations with similar results. **(d,e)** Drift corrected and dose filtered cryo-EM micrographs reveal clearly recognizable shapes for monomeric (d) and dimeric (e) particles. More than 10 grids have been prepared independently from more than three protein preparations with similar results. **(f)** Denaturating SDS-PAGE analysis with Coomassie staining of the sample used for cryo-EM grid preparation and data collection before SEC and after grid preparation.

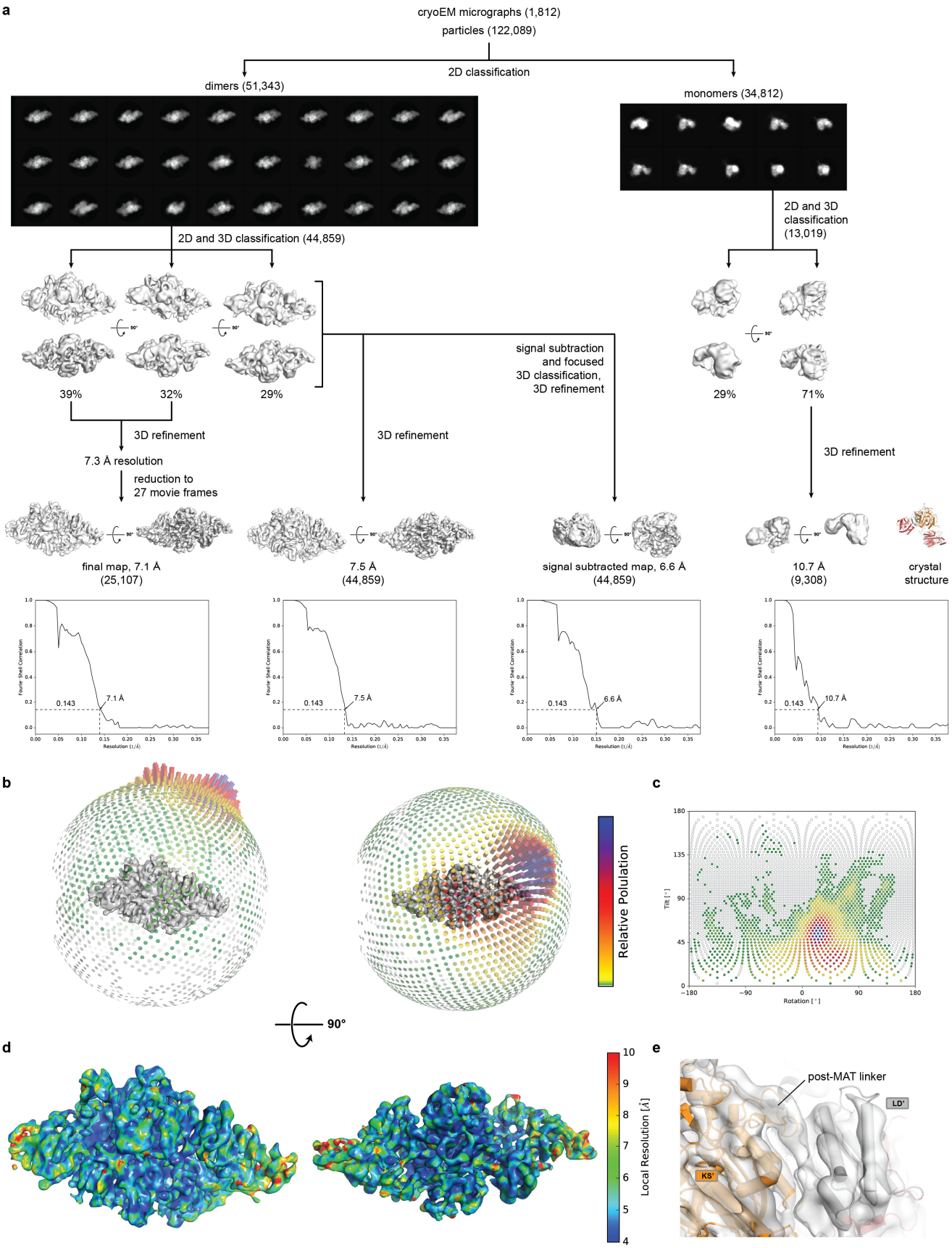
a
cryoEM micrographs (1,812)
particles (122,089)
2D classification
dimers (51,343)
monomers (34,812)
2D and 3D classification (44,859)
2D and 3D classification (13,019)
39%
32%
29%
29%
71%
3D refinement
7.3 Å resolution
reduction to 27 movie frames
3D refinement
signal subtraction and focused 3D classification, 3D refinement
3D refinement
final map, 7.1 Å (25,107)
7.5 Å (44,859)
signal subtracted map, 6.6 Å (44,859)
10.7 Å (9,308)
crystal structure
Fourier Shell Correlation
Resolution (1/Å)
0.143
7.1 Å
7.5 Å
6.6 Å
10.7 Å
b
90°
Relative Population
c
Tilt [°]
Rotation [°]
d
Local Resolution [Å]
e
post-MAT linker
LD'
KS'

Supplementary Figure 7 | Cryo-EM data processing scheme. **(a)** 2D- and 3D-classification and sorting scheme for reconstructions of CTB1 SAT°-KS-MAT°=ACP2 dimers as well as monomers. 3D-class distributions are indicated below the models. FSC plots (corrected for effects of the mask) used for determining resolution based on the 0.143 criterion (Rosenthal, P. B. & Henderson, R. J. Mol. Biol. 333, 721-745 (2003)) is shown below the final models. A single data set has been collected from one pre-screened protein and grid preparation. **(b, c)** 3D (b) and 2D (c) angular distribution plot based on the alignment used for the final reconstruction. **(d)** Local resolution map of the final reconstruction at 7.1 Å resolution shows a resolution below 5 Å in the central KS region, decreasing towards the lateral MAT domains to around 10 Å. **(e)** The final map reveals features of secondary structure elements as well as linkers. All maps are contoured at 7.1σ.

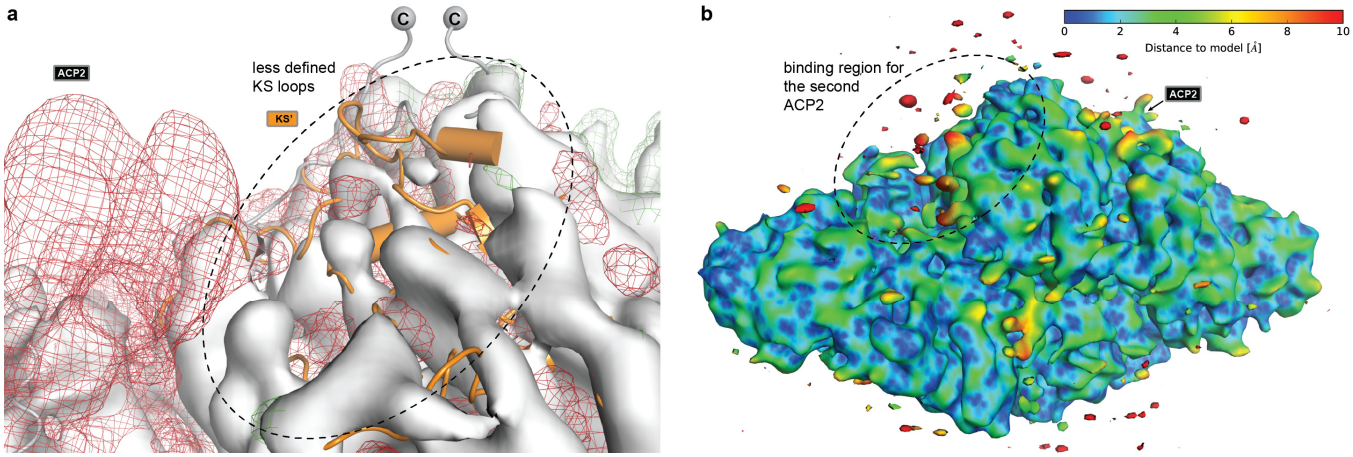

Supplementary Figure 8 | Conformational variability in the cryo-EM structure of CTB1 SAT^0-KS-MAT^0=ACP2. **(a**, **b)** KS-based C2 symmetry differences map of the final reconstruction at 7.1 Å resolution, contoured at 7.1σ (green: positive, red: negative). The potential ACP2 binding region on the KS surface is less ordered on the side lacking ACP2 density. **(b)** An unmasked map of the final reconstruction contoured at 3σ and colored by distance to the atomic model shows enhanced noise around the second ACP binding site.

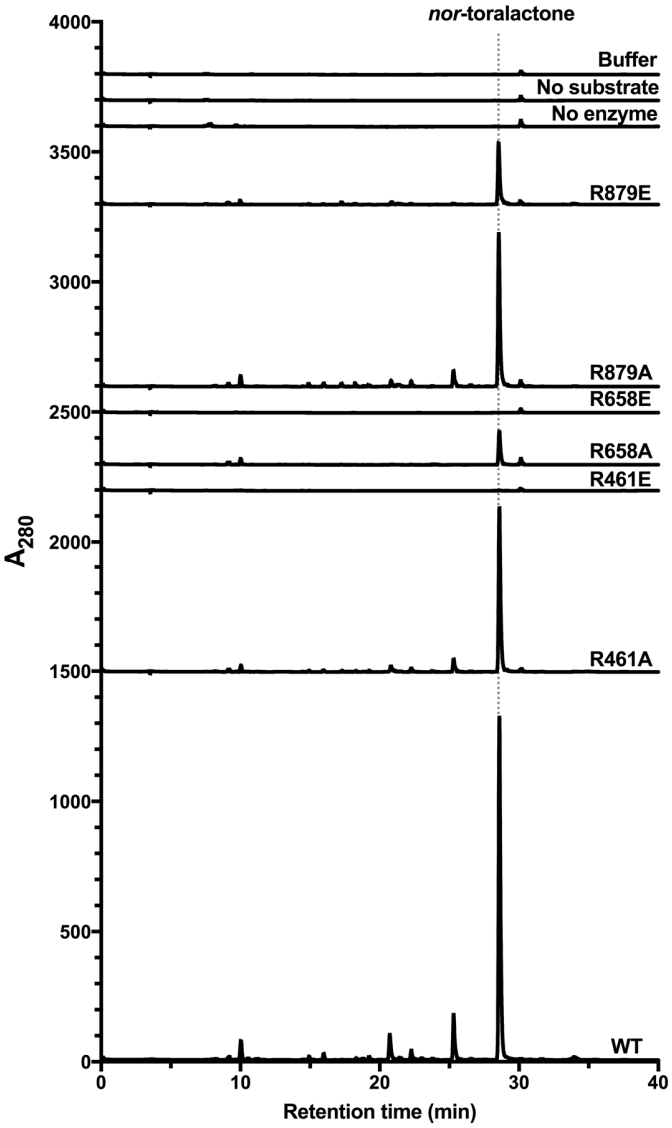

Supplementary Figure 9 | CTB1 mutant activity in deconstruction experiments and ACP2 interface validation. Representative HPLC chromatograms (280 nm) of full *in vitro* CTB1 reconstitution reactions (SAT-KS-MAT + ACP2 + PT + TE) with SAT-KS-MAT interface mutants are shown. Curves are off-set for visualization. *Nor*-toralactone production is indicated by a peak at a retention time of 28.6 min. These experiments were repeated three times with similar results.

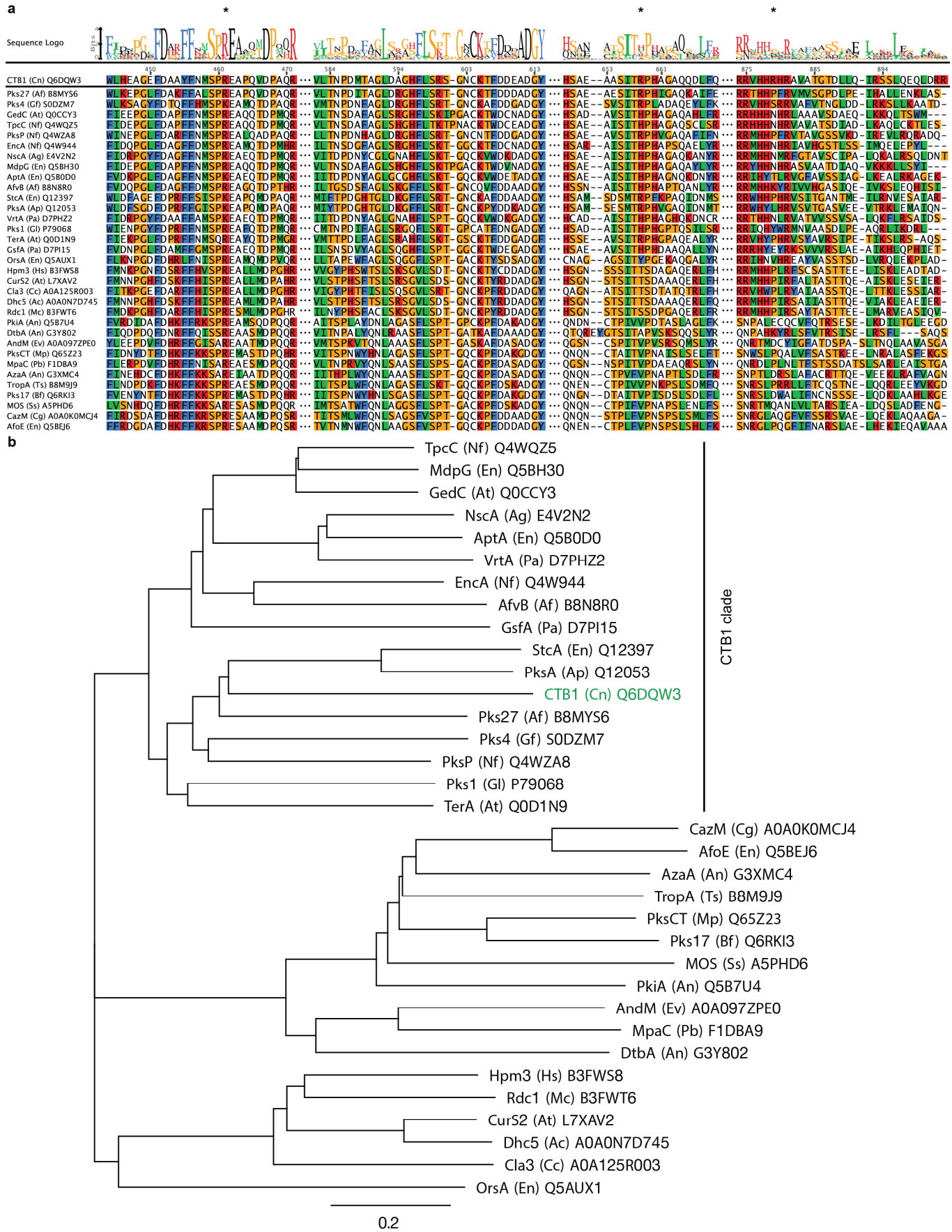
a
Sequence Logo
CTB1 (Cn) Q6DQW3
Pks27 (Af) B8MYS6
Pks4 (Gf) S0DZM7
GedC (At) Q0CCY3
TpcC (Nf) Q4WQZ5
PksP (Nf) Q4WZA8
EncA (Nf) Q4W944
NscA (Ag) E4V2N2
MdpG (En) Q5B8H30
AptA (En) Q5B0D0
AfvB (Af) B8N8R0
StcA (En) Q12397
PksA (Ap) Q12053
VrtA (Pa) D7PHZ2
Pks1 (Gl) P79068
TerA (At) Q0D1N9
GsfA (Pa) D7PI15
OrsA (En) Q5AUX1
Hpm3 (Hs) B3FWS8
CurS2 (At) L7XAV2
Cla3 (Cc) A0A125R003
Dhc5 (Ac) A0A0N7D745
Rdc1 (Mc) B3FWT6
PkiA (An) Q5B7U4
DtbA (An) G3Y802
AndM (Ev) A0A097ZPE0
PksCT (Mp) Q65Z23
MpaC (Pb) F1DBA9
AzaA (An) G3XMC4
TropA (Ts) B8M9J9
Pks17 (Bf) Q6RKI3
MOS (Ss) A5PHD6
CazM (Cg) A0A0K0MCJ4
AfoE (En) Q5BEJ6
b
TpcC (Nf) Q4WQZ5
MdpG (En) Q5BH30
GedC (At) Q0CCY3
NscA (Ag) E4V2N2
AptA (En) Q5B0D0
VrtA (Pa) D7PHZ2
EncA (Nf) Q4W944
AfvB (Af) B8N8R0
GsfA (Pa) D7PI15
StcA (En) Q12397
PksA (Ap) Q12053
CTB1 (Cn) Q6DQW3
Pks27 (Af) B8MYS6
Pks4 (Gf) S0DZM7
PksP (Nf) Q4WZA8
Pks1 (Gl) P79068
TerA (At) Q0D1N9
CTB1 clade
CazM (Cg) A0A0K0MCJ4
AfoE (En) Q5BEJ6
AzaA (An) G3XMC4
TropA (Ts) B8M9J9
PksCT (Mp) Q65Z23
Pks17 (Bf) Q6RKI3
MOS (Ss) A5PHD6
PkiA (An) Q5B7U4
AndM (Ev) A0A097ZPE0
MpaC (Pb) F1DBA9
DtbA (An) G3Y802
Hpm3 (Hs) B3FWS8
Rdc1 (Mc) B3FWT6
CurS2 (At) L7XAV2
Dhc5 (Ac) A0A0N7D745
Cla3 (Cc) A0A125R003
OrsA (En) Q5AUX1
0.2

Supplementary Figure 10 | CTB1 SAT-KS-MAT alignment of regions interfacing ACP2 and phylogeny. All sequences are labelled as "protein name (organism abbreviation) Uniprot number". **(a)** Sequence alignment of regions relevant for ACP2 interaction. *, indicates interface mutants that reduce activity. **(b)** Phylogenetic analysis of NR-PKS indicates three main clades with one clustering around CTB1. Distance unit is given as accepted amino-acid substitutions per site and indicated by scale bar.

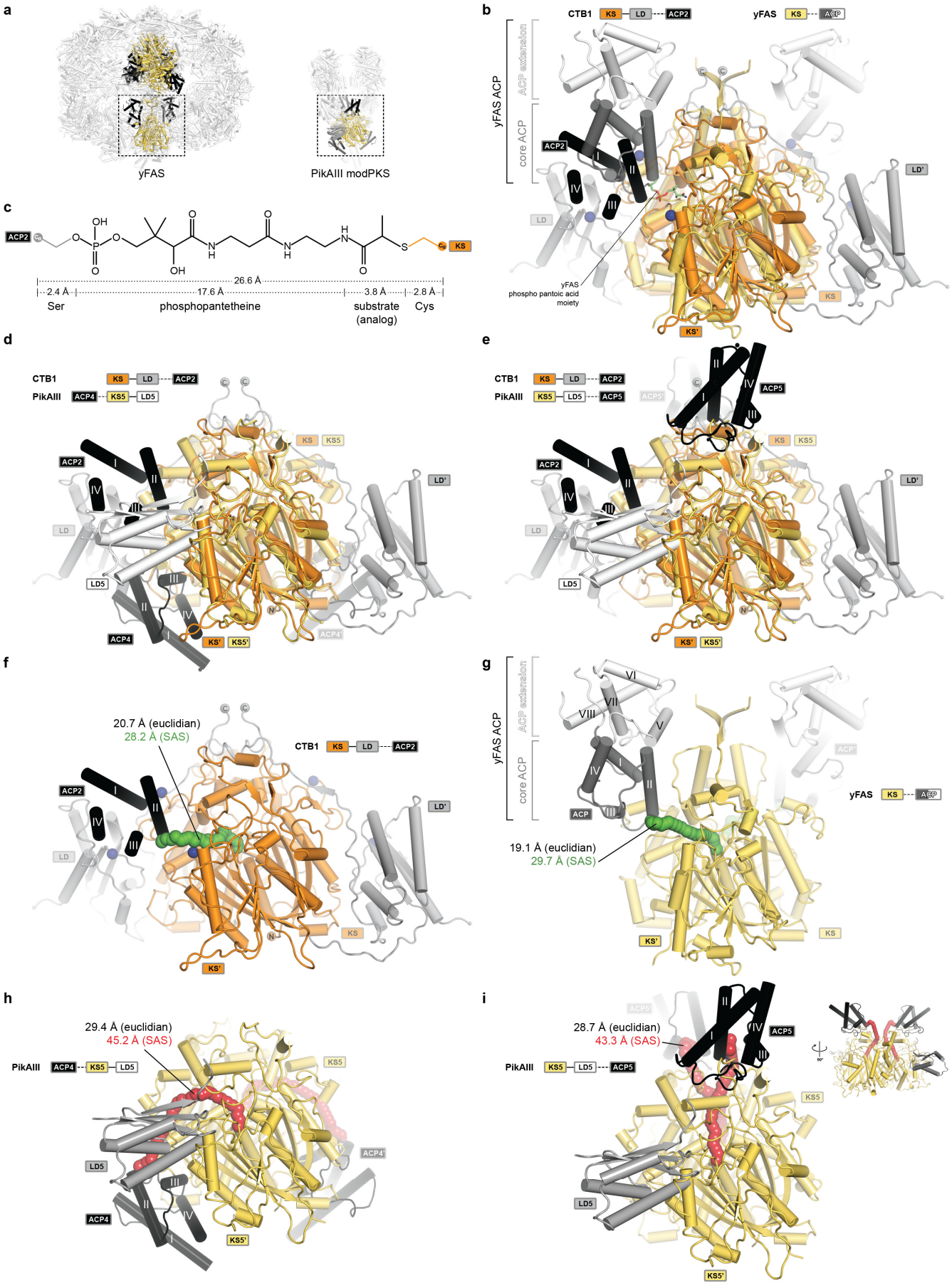
a
yFAS
PikAIII modPKS
b
CTB1
KS
LD
ACP2
yFAS
ACP
yFAS ACP
ACP extension
core ACP
LD'
yFAS
phospho pantoic acid
moiety
KS'
c
26.6 Å
2.4 Å
17.6 Å
3.8 Å
2.8 Å
Ser
phosphopantetheine
substrate
(analog)
Cys
d
PikAIII
ACP4
KS5
LD5
KS5'
e
ACP5
f
20.7 Å (euclidian)
28.2 Å (SAS)
g
19.1 Å (euclidian)
29.7 Å (SAS)
h
29.4 Å (euclidian)
45.2 Å (SAS)
i
28.7 Å (euclidian)
43.3 Å (SAS)

Supplementary Figure 11 | Comparison of KS-ACP interactions in PKS and FAS. **(a)** ACP interactions with multienzyme KS domains have been observed in the hetero-dodecameric yFAS and PikAIII modPKS. Superposition of the architecturally distinct yFAS-KS with CTB1 KS-LD°=ACP2. **(b)** The divergent ACP of yFAS consists of a *C*-terminal four-helix bundle extension (white) and the conserved four-helix bundle at the N-terminus, which interacts with the KS in a similar position as observed for ACP2 in CTB1. ACP-interfacing residues in CTB1 are indicated by blue spheres (see Fig. 3) **(c)** Derivation of the length of a fully extended crosslink between ACP2 and KS in CTB1. The defined length of the Ppant cofactor bridges a distance of approx. 27 Å between the ACP-Ser and the KS-Cys C_α atoms for functional ACP interaction with active sites. **(d, e)** Superpositions of PikAIII with ACP4 (d) and ACP5 (e) on CTB1 KS-LD=ACP2 show the relative locations of the ACP binding interfaces. The LD5 arrangement in PikAIII is invers to CTB1. **(f-i)** C_α-C_α solvent accessible surface (SAS) distances between the ACP anchor and the KS active site cysteine in CTB1 (f), yFAS (g), and PikAIII with ACP4 (h) and ACP5 (i) are indicated. Solvent accessible surface paths are indicated by tubes of spheres and colored according to the agreement (green) or disagreement (red) with the length of the Ppant cofactor. The path for ACP5 to KS5 in PikAIII (i) is only accessible in the absence of the post-(M)AT linker, which was not resolved in the cryo-EM structure. An additional miniaturized-sideview is indicated. Corresponding euclidian distances are given in the panels. Domain colors are indicated in the panels; only KS, LD, and ACP domains are shown (b-i).

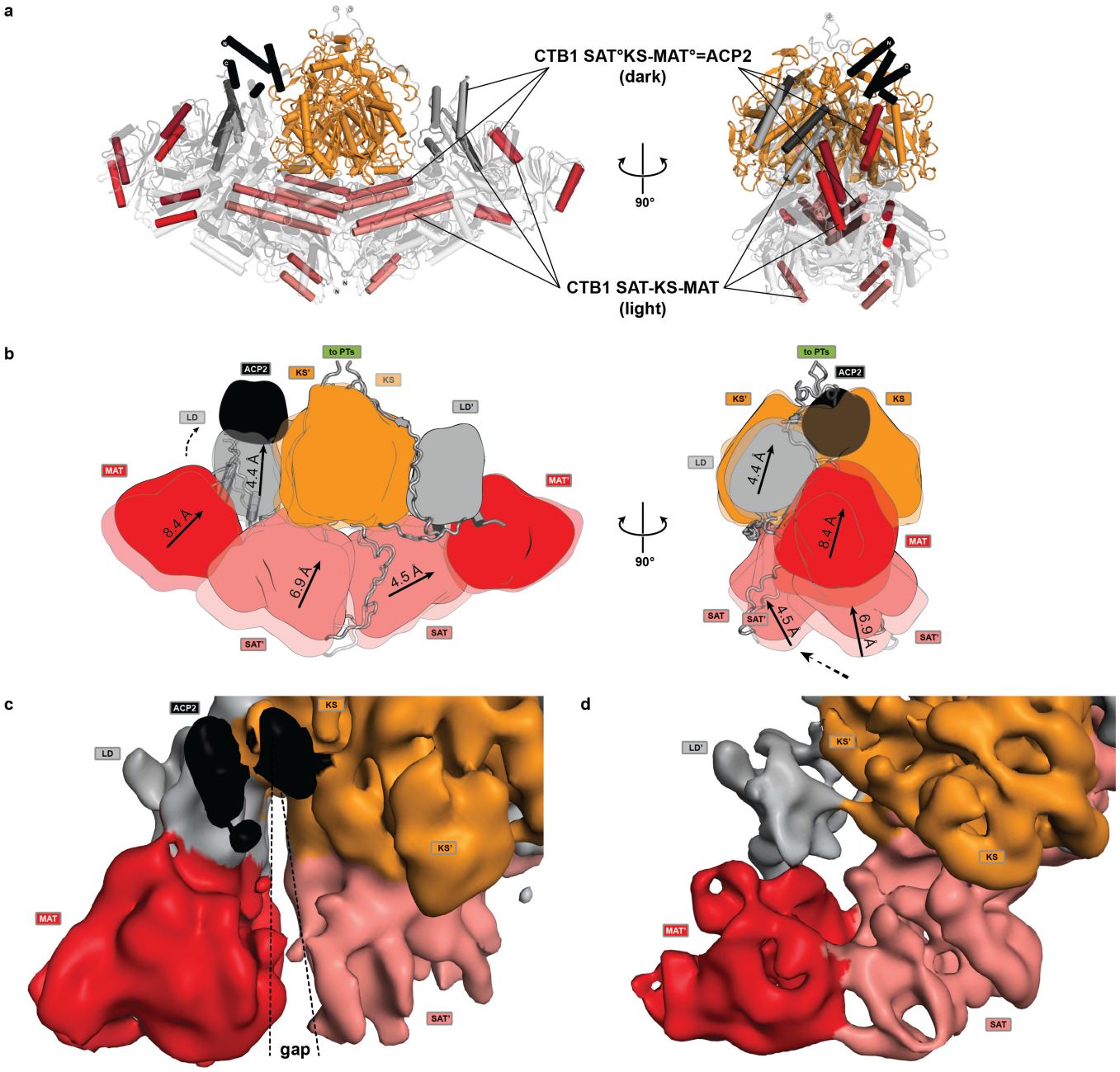

Supplementary Figure 12 | Structural comparison between CTB1 SAT-KS-MAT and SAT°-KS-AT°=ACP2. **(a)** Superposition on the central KS dimer. Transparent cartoon representation of CTB1 is shown in white (SAT-KS-MAT) and black (SAT°-KS-MAT°=ACP2). Selected helices are shown in light (SAT-KS-MAT) and dark (SAT°-KS-MAT°=ACP2) domain

colors. **(b)** Schematic representation of relative domain motions. Distances are derived by domain-wise C_α-r.m.s.d. calculations. **(c**, **d)** Structural differences at the MAT-SAT interface in the cryo-EM reconstruction are shown for the unsharpened map. While the side with visualized ACP2 (c) reveals a gap, the side with unresolved ACP2 shows a connected interface (d).

Supplementary Movie 1 | ACP2 binding to the CTB1 loading/condensing region. Structures of the CTB1 loading/condensing region with and without crosslinked ACP2 are morphed. In the ACP2-bound structure, ACP is visualized at a single binding-site in an overall structure with increased asymmetry. ACP2 is located in a cleft between the KS dimer and one LD. Around ACP2, LD and MAT are moved upwards, and the interface between the neighboring MAT and SAT domains is loosened. The SAT is translocated towards the KS and the second SAT is pushed against the KS and MAT in the opposite half of the dimer.